Estimating Topology Preserving and Smooth Displacement Fields

Bilge Karaçalı, *Member, IEEE* and Christos Davatzikos, *Member, IEEE*

***Abstract*—We propose a method for enforcing topology preservation and smoothness onto a given displacement field. We first analyze the conditions for topology preservation on two- and three-dimensional displacement fields over a discrete rectangular grid. We then pose the problem of finding the closest topology preserving displacement field in terms of its complete set of gradients, which we later solve using a cyclic projections framework. Adaptive smoothing of a displacement field is then formulated as an extension of topology preservation, via constraints imposed on the Jacobian of the displacement field. The simulation results indicate that this technique is a fast and reliable method to estimate a topology preserving displacement field from a noisy observation that does not necessarily preserve topology. They also show that the proposed smoothing method can render morphometric analysis methods that are based on displacement field of shape transformations more robust to noise without removing important morphologic characteristics.**

I. Introduction

In BIOMEDICAL image matching, a template is warped to a given patient scan in order to maximize point correspondences. The matching is expressed in terms of a displacement field $h : \Omega_T \rightarrow \Omega_I$, where Ω_T and Ω_I are the two-dimensional (2-D) or three-dimensional (3-D) domains of the template T and the patient scan I, respectively. Given a template and a patient scan, a displacement field h is determined usually by solving an energy minimization problem, where a cost function of form

$$E(h) = \int \left(F\left(I, h(\omega)\right) - F(T, \omega)\right)^2 d\omega + \Phi(h) \qquad (1)$$

is minimized through some iterative scheme. The term $(F(I, h(\omega)) - F(T, \omega))^2$ enforces data closeness, where $F(A, \omega)$ is a collection of descriptive features of image A at location ω. Frequently, $F(A, \omega)$ is chosen to be the brightness value of image A at ω, $A(\omega)$ [1], [5], [17]. More extensive feature representations have also been used with improved matching accuracy [19]. Regularity on the solution is enforced through $\Phi(h)$ which penalizes deviations from some measure of smoothness.

Another common approach to determine a displacement field h is to establish point correspondences between the template and the patient scan at a subset of points in the domain for which "reliable" point representations can be obtained [4], [9]. These values are then extrapolated over the rest of the domain to construct a complete displacement field.

The main intuition behind topology preservation in a displacement field is the desire to maintain connectivity between neighboring morphological structures. The template and the patient scan are presumably comprised of essentially the same components, dilated, shrunk, or translated at regions. Moreover, topology preservation is necessary for the invertibility of a transformation. The transformation that maps a template to an individual, for instance, should be invertible in order to allow mapping of the individual's images to a stereotaxic space, a process often called spatial normalization.

Whether a given deformation field preserves topology is usually monitored by the determinant of the Jacobian over the domain. In a 2-D setting, a deformation field h can be expressed in terms of its Cartesian components as $h = (f, g)$, where $f : \Omega \rightarrow \mathbb{R}$ and $g : \Omega \rightarrow \mathbb{R}$ denote its value over the x and y axes. The determinant of the Jacobian of h at $(x, y) \in \Omega \subset \mathbb{R}^2$, denoted by $J_h(x, y)$ and referred briefly to as its Jacobian, is computed using

$$J_h(\omega) = \begin{vmatrix} \frac{\partial f}{\partial x}(x, y) & \frac{\partial f}{\partial y}(x, y) \\ \frac{\partial g}{\partial x}(x, y) & \frac{\partial g}{\partial y}(x, y) \end{vmatrix}. \qquad (2)$$

Topology preservation in image matching can then be enforced on the estimated displacement field minimizing (1) by ensuring positivity on the Jacobian $J_h(\omega)$ at every iteration through selections of hard [5], [17] or soft constraints [1] using the properties of the selected model for h. A practical alternative to such continuous monitoring of $J_h(x, y)$ is to enforce displacement field characteristics associated with a positive Jacobian such as invertibility [13], [20], which, however, does not mathematically guarantee preservation of topology.

Christensen *et al.* [5] propose a fluid model representation for deformations to bring two morphologies into correspondence. The advantage of the model is that the deformations expressed as such inherently preserve topology by construction. The registration problem is then solved by numerical approximations to fluid diffusion. On the other hand, there is no guarantee that the morphological variations across subject anatomies is well approximated by a fluid model deformation.

The approach of Ashburner *et al.* considers a triangular partition of a 2-D domain and characterize the Jacobian determinant on the triangles, but is biased toward the direction of diagonalization. In this approach, a square patch is partitioned into two triangles, but the deformation of diagonal vertices are treated differently, whereas our results show that this characterization is incomplete. Completing this approach would require a second triangulation along the opposite diagonal. Furthermore, the approach is limited to 2-D cases.

Manuscript received October 29, 2003; revised March 10, 2003. The Associate Editor responsible for coordinating the review of this paper and recommending its publication was J. Pluim. *Asterisk indicates corresponding author*.

*B. Karaçaı is with the Section of Biomedical Image Analysis, Department of Radiology, University of Pennsylvania, Philadelphia, PA 19104 USA (e-mail: bilge@rad.upenn.edu).

C. Davatzikos is with the Section of Biomedical Image Analysis, Department of Radiology, University of Pennsylvania, Philadelphia, PA 19104 USA.

Digital Object Identifier 10.1109/TMI.2004.827963

Musse *et al.* derive the topology preservation conditions for 2-D deformation fields, but do not address their analogs in a 3-D case. Moreover, their characterization of the Jacobian determinant is valid only when their interpolating spline is of order one, i.e., linear. For higher order interpolants, the tail interferes with the neighboring deformations and the Jacobian determinant becomes dependent on neighboring deformations as well. Nonlinear interpolants also produce curved boundaries between the deformations of adjacent squares that violate the convexity argument that leads to topology preservation. Algorithmically, their method relies on the fact that at the beginning of an iteration, a (2-D) deformation field that satisfies topology preservation conditions (in two dimensions) is available, and finds a desirable update that improves an image similarity measure as the registration is performed. Then, the prescribed deformation updates are sequentially evaluated separately at every point in a way to still satisfy the topology preservation conditions which involve that particular point. This strategy disregards the fact that deformations on other points also affect the very conditions under consideration and, thus, the "corrected" modifications are biased to the order of sequential processing and are not the set of modifications truest to the ones prescribed by the registration.

In 2-D deformations, our approach enforces essentially the same set of conditions for topology preservation given that the interpolation is linear (the mathematics are invariant to the development), but we perform deformation corrections by processing all the deformations simultaneously to enforce these conditions on the deformation gradients as opposed to deformations themselves. This way, we can claim that the conditions are enforced by considering deformations on all points and by finding the best tradeoff. We then extend the development for correcting 3-D deformations for topology preservation.

We consider enforcing topology preservation as a hard constraint at several intermediate steps of a deformable registration procedure or after the registration is done. Enforcing topology preservation during registration as suggested in the literature restricts the deformation field estimation scheme to a few models for which constraining the positivity of the Jacobian is feasible. It is, however, well known that some models work well in some applications, but do not perform reasonably in others. Furthermore, these models generally employ an improvised set of criteria through numerical approximations. Our development focuses on deriving the exact and optimal criteria for topology preservation given a pixel- or voxel-wise registration problem. These criteria are then administered to a given deformation field by our method which undoes the folds that violate the topology preservation. The analysis indicates that smoothing mechanisms embedded in registration schemes are unreliable to the end of achieving a topology preserving mapping between two subjects; for topology preserving mappings need not be smooth, and smooth mappings need not be topology preserving.

The developed topology preservation scheme also provides an adaptive deformation field regularity mechanism by means of limiting the Jacobian determinants to within a neighborhood of $1.0 \in \mathbb{R}$. This neighborhood can also be centered on any positive real number by scaling the partial derivatives with a proper factor. In contrast to conventional schemes that achieve regularity by smoothing the deformation field, this technique achieves deformation field regularity by explicitly limiting the amount of contraction and expansion measured by the Jacobian determinants. Simulation results demonstrate that the method not only moderates the deformation field behavior in an effective and direct manner, it also improves the accuracy and generalizability of the registration.

In this paper, we provide a detailed analysis of a generic algorithm to enforce topology preservation on a given deformation field we have introduced earlier with some preliminary results [14]. We first present a description of deformation field properties in conjunction with the corresponding Jacobian and its determinant. The next section is devoted to the analysis of the mathematical relationship between a deformation field and the values of its Jacobian determinant over continuous and discrete image domains. In Section III, we describe a technique to determine a topology preserving and regular displacement field closest (in some sense) to a given (noisy) displacement field, and present simulation results in Section IV.

II. Methodology

A. Continuous Domain Formulation

In order for a continuously differentiable deformation field to preserve topology, its Jacobian needs to be positive everywhere in its domain. Conversely, it can be shown [17] that if a deformation field is continuous and globally one-to-one, it also preserves topology. Neither of these, however, applies to deformation fields that are defined over a discrete grid of points.

When we speak of topology preservation conditions to be satisfied by a discrete deformation field h, we refer to the topology preserving nature of the continuous deformation field h_c obtained by a bilinear interpolation of the discrete deformation field. Since such an interpolation is not guaranteed to be continuously differentiable everywhere, we approach the topology preservation issue with regard to the continuity and globally one-to-one properties. By construction, h_c is continuous. Globally one-to-one properties, on the other hand, are conditional on the local behavior of h_c which are governed by h. Specifically, if the continuous deformation field h_c is one-to-one over all square/cubic patches that partition the continuous domain defined by the discrete grid, then h_c is globally one-to-one.

We address topology preservation conditions in 2-D and 3-D settings separately below. While the essential principle is common between the two cases, feasibility considerations suggest replacing a computationally expensive but definite set of sufficient conditions with approximate but computationally feasible ones.

B. Topology Preservation in Two Dimensions

We first state a result that establishes topology preservation conditions for a deformation field that defines correspondences between two domains that are both subsets of $\mathbb{Z}^2$ [14].

Lemma 1: Let $p_1 = (x_0, y_0)$, $p_2 = (x_0 + 1, y_0)$, $p_3 = (x_0, y_0 + 1)$, $p4 = (x_0 + 1, y_0 + 1)$, $p_1, p_2, p_3, p_4 \in \Omega =$

$[0,\ldots,M-1]\times[0,\ldots,N-1]$, and $h:\Omega\rightarrow\mathbb{R}^2$ a discrete deformation field with $h=(f,g)$. Define the forward and backward approximations to partial derivatives of f (and similarly for g) at (x,y) as

$$\begin{aligned} f_x^f(x,y)&=f(x+1,y)-f(x,y)\\ f_y^f(x,y)&=f(x,y+1)-f(x,y)\\ f_x^b(x,y)&=f(x,y)-f(x-1,y)\\ f_y^b(x,y)&=f(x,y)-f(x,y-1). \end{aligned}$$

Then, the following statements are equivalent.

1) The four possible approximations to the Jacobian of h in the square patch defined by p_1, p_2, p_3, and p_4, given by

$$\begin{aligned} J^{ff}&=f_x^f(p_1)g_y^f(p_1)-f_y^f(p_1)g_x^f(p_1)\\ J^{bf}&=f_x^b(p_2)g_y^f(p_2)-f_y^f(p_2)g_x^b(p_2)\\ J^{fb}&=f_x^f(p_3)g_y^b(p_3)-f_y^b(p_3)g_x^f(p_3)\\ J^{bb}&=f_x^b(p_4)g_y^b(p_4)-f_y^b(p_4)g_x^b(p_4) \end{aligned}$$

   are positive.
2) The angles defined by $(h(p_3),h(p_1),h(p_2))$, $(h(p_1),h(p_2),h(p_4))$, $(h(p_2),h(p_4),h(p_3))$, and $(h(p_4),h(p_3),h(p_1))$ are between 0 and π.
3) The signed area of the triangles defined by $(h(p_3),h(p_1),h(p_2))$, $(h(p_1),h(p_2),h(p_4))$, $(h(p_2),h(p_4),h(p_3))$, and $(h(p_4),h(p_3),h(p_1))$ given by

$$A_{h(p_3),h(p_1),h(p_2)}=\frac{1}{2}\begin{vmatrix}1 & f(p_3) & g(p_3)\\ 1 & f(p_1) & g(p_1)\\ 1 & f(p_2) & g(p_2)\end{vmatrix}.$$

   and similarly for $A_{h(p_1),h(p_2),h(p_4)}$, $A_{h(p_2),h(p_4),h(p_3)}$, and $A_{h(p_4),h(p_3),h(p_1)}$, are positive.

The proof which is solely based on algebraic manipulations is omitted. The equivalence of these statements is illustrated in Fig. 1. The significance of the sign information of the triangle areas lies in the counter-clockwise ordering of the points, which is violated when the corresponding angle goes beyond the interval $(0,\pi)\subset[0,2\pi)$.

Definition 1: Let $\mathcal{C}$ be the class of deformation fields $h=(f,g)$ defined over a discrete rectangular grid $\Omega=[0,\ldots,M-1]\times[0,\ldots,N-1]\subset\mathbb{Z}^2$ for which J^{ff}, J^{fb}, J^{bf}, and J^{bb} are positive at all $(x,y)\in\Omega$.

Proposition 1: Let a deformation field $h=(f,g)$ defined over a discrete rectangular grid $\Omega=[0,1,\ldots,M-1]\times[0,1,\ldots,N-1]\subset\mathbb{Z}^2$ be an element of $\mathcal{C}$. Then, its continuous counterpart determined via the interpolation of h over the domain $\Omega_c=[0,M-1]\times[0,N-1]\subset\mathbb{R}^2$ using the (bilinear) interpolant $\phi(x,y)$ given by

$$\phi(x,y)=\phi(x)\phi(y) \tag{3}$$

with

$$\phi(t)=\begin{cases}1+t, & \text{if } -1\le t<0\\ 1-t, & \text{if } 0\le t<1\\ 0, & \text{otherwise}\end{cases} \tag{4}$$

preserves topology over Ω_c.

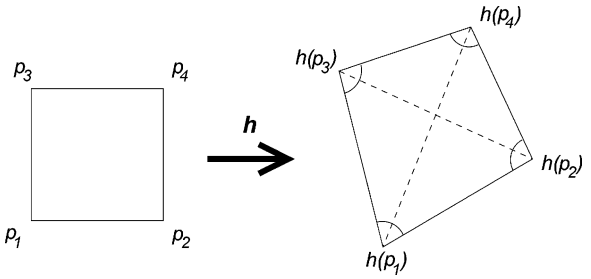

Fig. 1. Illustration of the equivalent statements of Lemma 1. Convexity of the region is violated when the images of the points cross over the diagonal connecting their neighbors. The corresponding angle exceeds π, and the counter clockwise order of the points in the triangle changes. Consequently, the area of the triangle computed by the determinant changes sign and becomes negative.

Proof: Consider the behavior of h_c over the square patch S defined by $p_1=(x_0,y_0)$, $p_2=(x_0+1,y_0)$, $p_3=(x_0,y_0+1)$, $p4=(x_0+1,y_0+1)$, $p_1,p_2,p_3,p_4\in\Omega=[0,\ldots,M-1]\times[0,\ldots,N-1]$. Expanding the expression for the Jacobian determinant inside S reveals that it is expressed as a convex sum of the 4 corner Jacobians J^{ff}, J^{fb}, J^{bf}, and J^{bb}. Since these are all positive by the hypothesis, so is the Jacobian everywhere inside S. Continuity of the bilinear interpolant provides continuity of h_c over S, and hence, h_c is locally one-to-one over all such S, and globally one-to-one over Ω_c. This completes the proof. ■

C. Topology Preservation in Three Dimensions

The derivation for these conditions is identical to the 2-D case, except that the conditions now involve partial derivative approximations that are not all embodied by a corner of a cubic patch, as opposed to having a direct correspondence between corner Jacobians and the set of all Jacobians inside a cubic patch. Namely, the number of Jacobians that manifest inside a cubic patch is 64, among which only 8 are the corner Jacobians. A detailed analysis on the representation of the Jacobian determinant inside a cubic patch in terms of these 64 Jacobians is presented in the Appendix.

Proposition 2: Let a deformation field $h=(f,g,e)$ defined over a discrete rectangular grid $\Omega=[0,1,\ldots,M-1]\times[0,1,\ldots,N-1]\times[0,1,\ldots,K-1]\subset\mathbb{Z}^3$ be such that all 64 Jacobians are positive over all cubic patches in Ω. Then, its continuous counterpart determined via the interpolation of h over the domain $\Omega_c=[0,M-1]\times[0,N-1]\times[0,K-1]\subset\mathbb{R}^3$ using the (trilinear) interpolant $\phi(x,y,z)$ given by

$$\phi(x,y,z)=\phi(x)\phi(y)\phi(z). \tag{5}$$

Proof: The proof follows exactly the development for the 2-D case. ■

Note that with the extension from two dimensions to three, dimensions the number of topology preservation conditions increase from 4 to 64. Establishing and enforcing positivity of 64 Jacobians per cubic patch can be quite tedious, especially in cases where the discrete domain is comprised of a few thousands of cubic patches. Therefore, we approximate these complete 3-D topology preservation conditions by bounding the 8 corner Jacobians from below by a lower bound greater than zero.

The main reason that makes the corner Jacobians special is the mere fact that they are the only ones that are derived from

partial derivative approximations common to a certain point: the limiting value of the continuous Jacobian at a point inside a cubic patch as the point approaches a corner is 1 of these 8 corner Jacobians. The others correspond to derivative approximations that mix and match partial derivatives between corner differences that do not share a common voxel. These Jacobians, therefore, never materialize anywhere inside the cubic patch. Furthermore, for the most part, enforcing positivity of these 8 corner Jacobians does indeed suffice to enforce positivity of all 64 Jacobians. It should be noted that positivity of corner Jacobians is necessary for topology preservation inside a cubic patch: if only one of them is negative, there will be an open set inside the patch with positive measure over which the Jacobian determinant of the continuous deformation field is negative due to its continuity in terms of the Cartesian coordinates. On the other hand, positivity of all 64 Jacobians is sufficient for topology preservation, but that sufficiency does not entail necessity; for topology preservation can be held without having all 64 Jacobians positive.

The efficacy at which the values of the corner Jacobians impose a given structure onto a deformation field can be demonstrated in other instances, like simulation of atrophy in brain tissue. The values of corner Jacobians correspond to a factor of the tetrahedral volumes at the corresponding vertices of the given cubic patch, which are strongly tied to the volume of the cube after deformation. It is then possible to simulate volume loss by imposing corner Jacobians to attain a suitable set of values, and seeking a deformation that achieves these prescribed corner Jacobians. This can be done by minimizing a cost function of the form

$$E(h) = \frac{1}{2} \sum_{x,y,z} \sum_{i=1}^{8} \left(J_i(x,y,z) - J_i^T(x,y,z) \right)^2 \qquad (6)$$

where $J_i^T(x,y,z)$ is the desired value for the corner Jacobian i of the cubic patch (x,y,z), $J_i(x,y,z)$ is the respective corner Jacobian produced by the deformation field h, and the deformation h is the variable of optimization. A very localized brain tissue atrophy can, thus, be obtained by setting the target Jacobians over the gray matter and the white matter to a desired level such as 0.85 for a 15% atrophy, or 0.50 for a 50% atrophy, and compensating for the volume loss by increasing the Jacobians over the cerebro-spinal fluid by an adequate amount. Fig. 2 illustrates a highly localized atrophy on a segmented volume of an actual human brain. This demonstrates the amount of control that the corner Jacobians have on the underlying deformation.

III. Proposed Approach

Now that we have the set of conditions for a discrete deformation field to satisfy in order to produce a topology preserving continuous counterpart after linear interpolation, we proceed to describe an iterative algorithm that enforces these conditions on a given deformation field with minimal correction. We first visit the continuous domain formulation in order to derive a method to correct a continuous deformation field for topology preservation. We will then apply the same principle to enforce the topology preservation conditions onto a discrete deformation field.

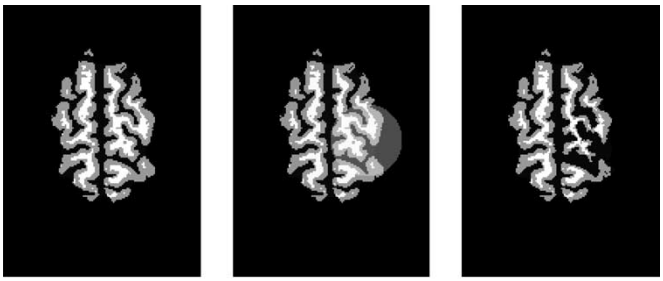

Fig. 2. Simulation of 50% brain atrophy on a segmented volume of a human brain, only the axial slices shown. A slice of the original volume is shown in (a) where the white matter, the gray matter and the cerebro-spinal fluid are painted in a descreasing order of brightness. Simulation of tissue atrophy is performed by setting the corner Jacobians in the designated region in (b) to 0.5 over the brain tissue, and to an accordingly increased level over the cerebro-spinal fluid. Warping the original volume by the obtained deformation results in a brain with atrophy in (c).

Let a continuous deformation field h be given with Cartesian components f, g, and e, respectively, along x, y, and z axes

$$f(x,y,z) = x + \tilde{f}(x,y,z) \qquad (7)$$
$$g(x,y,z) = y + \tilde{g}(x,y,z) \qquad (8)$$
$$e(x,y,z) = z + \tilde{e}(x,y,z) \qquad (9)$$

where $\tilde{f}$, $\tilde{g}$, and $\tilde{e}$ are the corresponding displacement field components. Suppose that at a point (x,y,z), this deformation field bears a Jacobian determinant denoted by $J(x,y,z)$. Now, define another deformation field, h_α, with Cartesian components f_α, g_α, and e_α defined as

$$f_\alpha(x,y,z) = x + \alpha\tilde{f}(x,y,z) \qquad (10)$$
$$g_\alpha(x,y,z) = y + \alpha\tilde{g}(x,y,z) \qquad (11)$$
$$e_\alpha(x,y,z) = z + \alpha\tilde{e}(x,y,z). \qquad (12)$$

Let $J_\alpha(x,y,z)$ denote the determinant of the Jacobian of h_α at the point (x,y,z). It is then easy to see that

$$\lim_{\alpha\to 0} J_\alpha(x,y,z) = 1 \qquad (13)$$
$$\lim_{\alpha\to 1} J_\alpha(x,y,z) = J(x,y,z). \qquad (14)$$

Suppose now, that $J(x,y,z) < 0$, which violates continuous topology preservation conditions. From the continuity of $J_\alpha(x,y,z)$ with respect to α, there exists $\alpha^\star \in [0,1]$ such that $J_{\alpha^\star}(x,y,z) = \epsilon > 0$ with $\epsilon <= 1$. Similarly, if $J(x,y,z)$ is larger than a preset threshold ϵ', we are guaranteed that there exists another $\alpha^\star \in [0,1]$ such that $J_{\alpha^\star}(x,y,z) = \epsilon'$. Consequently, by solving for $\alpha^\star$ given $h(x,y,z)$ and $J(x,y,z)$, we can bring the Jacobian determinant to a bounded interval around zero. Positivity of the Jacobian is then easily achieved by choosing a positive lower bound less than one to obtain a topology preserving mapping [14].

Confining the Jacobian values to a positive interval has an additional benefit. Jacobian determinants that are very small are associated with strong contractions on the mapping, while large values indicate strong expansions. Conventionally, for the sake of estimation validity and generalizability, these strong features have been dealt with through the indirect and imprecise way of smoothing the displacement fields [3], [12]. Limiting the Jacobian determinants from below and above with suitable lower and

upper bounds achieves this regularity by directly and explicitly limiting the unit contractions and expansions on the mapping. In addition, regularity obtained as such is adaptive in nature, since the expansions and contractions are adjusted with an indirect regard to how smooth the deformation itself is: as long as the bounds on the Jacobians are satisfied, the deformation field can have sharp features and exhibit rapid changes. Smoothness is neither necessary nor sufficient for topology preservation [14]. A further level of adaptivity can be achieved by considering spatially varying lower and upper bounds in conjunction with a statistical variability atlas of some sort, but for the purposes of this paper, we content with universal bounds on the Jacobian determinants.

Applying this scheme onto discrete settings is another story: over a continuum, the partial derivatives and, hence, the Jacobians are unique. On the other hand, there are more than one partial derivative approximations that produce their own Jacobian determinants which have individually to be within the prescribed bounds. Since there is a one-to-one correspondence between the Jacobian determinants and the partial derivatives of a discrete deformation field, we apply the Jacobian correction scheme described above to the gradient fields of the deformation fields, and not onto the deformation fields themselves. As a result, we compute the full set of gradient fields from a given deformation field, one for each kind of Jacobian, correct them over the entire domain, and reconstruct a corrected deformation field from these modified gradient fields.

In order to reconstruct a deformation field from its gradients, we use an algorithm proposed earlier by Karacali and Snyder [15], [16]. In the absence of modifications, recomputing the deformation field from its gradients is a straightforward sum along arbitrary paths. The corrections enforced by topology preservation, on the other hand, impact the desired accord between the gradients so that the result of integration now depends on the integration path. This is characterized as the loss of integrability of the gradient fields. The method in [15] provides a minimum norm solution to reconstructing a function from its gradient fields as a vector projection in the gradient space. As the details of this method are secondary to our analysis, we include them in the Appendix.

We can now summarize the requirements on the deformation field gradients to produce discrete deformation fields that satisfy the topology preservation conditions as

- the gradient fields have to generate positive Jacobians;
- the gradient fields have to be integrable.

This suggests a projection onto convex sets [7], [21], type of approach, where a *feasible* solution is found by repeatedly *projecting* the solution at a given iteration onto the subsets of the solution space which characterize these two conditions. In other words, starting at an initial solution, such a set-theoretic approach finds a solution that satisfies both of the requirements. Furthermore, if the property sets of these requirements are closed and convex, the solution obtained is indeed the projection of the initial solution onto the intersection of the property sets and, hence, the optimal solution. In this case, the property set of the second requirement is a subspace in the space of gradient fields, and hence, convex. The first property set, on the other hand, is not, since one can find pathological cases where the average of two topology preserving deformation fields is not topology preserving. One such example is a deformation field characterized by a 180° of rotation. The solution obtained by this approach is, therefore, not guaranteed to be the optimal solution. The simulation results presented next, however, indicate that it is reasonably close, and much better than other alternative schemes.

A step-by-step description of the algorithm that enforces topology preserving regularity on a given 3-D deformation field then goes as follows:

1) given initial deformation field $h = (f, g, e)$, and the desired bounds on the corner Jacobians ϵ_1 and ϵ_2;
2) let $f^{(0)} = f$, $g^{(0)} = g$, $e^{(0)} = e$;
3) compute the gradient fields $f_x^{(0)}$, $f_y^{(0)}$, $f_z^{(0)}$ from $f^{(0)}$;
4) compute the gradient fields $g_x^{(0)}$, $g_y^{(0)}$, $g_z^{(0)}$ from $g^{(0)}$;
5) compute the gradient fields $e_x^{(0)}$, $e_y^{(0)}$, $e_z^{(0)}$ from $e^{(0)}$;
6) compute the corner Jacobians J^{fff}, J^{ffb}, J^{fbf}, J^{fbb}, J^{bff}, J^{bfb}, J^{bbf}, J^{bbb};
7) while the extrema of the Corner Jacobians exceeds the interval $[\epsilon_1\ \epsilon_2]$, do for $k = 1, 2, \ldots$:
   a) for all corner Jacobians outside the bounds:
      i) find the gradient combination corresponding to the Jacobian;
      ii) correct the gradient combination so that the Jacobian is within $[\epsilon_1\ \epsilon_2]$;
   b) enforce integrability on the corrected gradients to obtain $f_x^{(k+1)}$, $f_y^{(k+1)}$, $f_z^{(k+1)}$, $g_x^{(k+1)}$, $g_y^{(k+1)}$, $g_z^{(k+1)}$, $e_x^{(k+1)}$, $e_y^{(k+1)}$, and $e_z^{(k+1)}$;
   c) compute the corner Jacobians J^{fff}, J^{ffb}, J^{fbf}, J^{fbb}, J^{bff}, J^{bfb}, J^{bbf}, and J^{bbb};
8) integrate $f_x^{(k+1)}$, $f_y^{(k+1)}$, and $f_z^{(k+1)}$ to obtain $\hat{f}$;
9) integrate $g_x^{(k+1)}$, $g_y^{(k+1)}$, and $g_z^{(k+1)}$ to obtain $\hat{g}$;
10) integrate $e_x^{(k+1)}$, $e_y^{(k+1)}$, and $e_z^{(k+1)}$ to obtain $\hat{e}$;
11) increase $\hat{f}$ by a constant so that its mean equals that of f;
12) increase $\hat{g}$ by a constant so that its mean equals that of g;
13) increase $\hat{e}$ by a constant so that its mean equals that of e.

The algorithm for the 2-D case is virtually identical to, and can easily be deduced from the 3-D case.

Note that this algorithm and its 2-D counterpart correct given 2-D or 3-D deformation fields for topology preserving regularity, by confining their corner Jacobians to within a prescribed set of upper and lower bounds. They can be applied to deformation field estimates obtained at intermediate steps of a deformable registration scheme as well as the final deformation estimate.

IV. Simulation Results

In this section, we present a set of results on simulated and real data that demonstrate the capabilities of the proposed technique. An earlier work [14] had shown that the proposed algorithm to regularize a given deformation field was confining the Jacobian values to within a prescribed interval with much less correction than an alternative Gaussian regularizer. The set of simulations and experiments we present here are aimed at analyzing the convergence properties of the algorithm as well

as application to a medical data characterization problem and implementation to regular size actual deformation fields that register a group of magnetic resonance imaging (MRI) scans to a brain template.

The following set of simulations compare the performances of serial and parallel implementations of the set-theoretic technique to enforce topology preservation conditions on a given deformation field in comparison with two reciprocal algorithms from the literature [8]. Then, we perform a convergence analysis of the serial implementation that illustrates the behavior of the proposed method in increasingly nontopology preserving conditions. Finally, we apply the algorithm to synthetic and real medical images using the optimal block processing strategy.

A. Performance Comparison of Various Implementations of the Proposed Technique

The set-theoretic framework of the topology-preserving deformation field estimation method can be implemented in various ways, each with its own set of advantages and disadvantages regarding convergence rate, properties of the solution, and response in pathological conditions. One such implementation is a serial implementation, where an initial point is repeatedly *projected* onto the property sets one at a time in a cyclic order. Another implementation is parallel in nature, where the next iteration solution is determined by a weighted average of the *projections* onto individual property sets, which is usually the arithmetic average. Modifications of these two basic principles have been proposed [8] and shown to converge to the optimal solution conditional on some convexity arguments, which we refer to as the *optimal serial* and *optimal parallel* implementations.

We have randomly generated a nontopology preserving deformation field on a 16×16 discrete regular grid, and used the serial, parallel, optimal serial and optimal parallel implementations of the proposed technique to recover topology preserving mappings. The original deformation field h with a minimum Jacobian value of -5.7559 is shown in Fig. 3. The reconstructed deformation fields h_s, h_p, h_{os}, and h_{op} obtained, respectively, by the serial, parallel, optimal serial, and optimal parallel algorithms are shown in Fig. 4. The value of ϵ is set to 0.1, and the iterations were stopped when the minimum value of the Jacobians exceeded $\epsilon/2 = 0.05$.

The statistics of the reconstructions are shown in Table I. The serial algorithm achieves the fastest convergence at an accuracy closely matching those of the optimal algorithms, and emerges as the most practical approach to the problem of enforcing topology preservation on an arbitrary deformation field. The main reason underlying this empirical result is the adaptive nature of the correction imposed on the gradient fields by the transformation T: at every iteration, only the gradients at points where the Jacobians are less than ϵ are corrected with minimal distortion. The resulting algorithm, hence, produces a result with smallest deformity to the initial displacement field.

B. Convergence Analysis of the Serial Implementation

In order to analyze the convergence properties, we have applied the serial implementation to a collection of random deformation fields, where the displacement fields $n_x = f - x$ and $n_y = g - y$ are assigned according to a zero-mean Gaussian distribution with varying standard deviations denoted by σ which controls the strength of the deformation. The statistics in Table II represent the average values of initial and final Jacobian minimums, the number of iterations until convergence, and the cost function $H(f)$ defined by

$$H(h) = \frac{1}{2} \sum_x \left\| h(x) - \bar{h}(x) \right\|^2 \tag{15}$$

obtained from 20 independent runs for every value of $\sigma = 0.25, 0.50, 0.75, \ldots, 3.00$. In (15), $\bar{h}$ denotes the given, not necessarily a topology preserving deformation.

The inverse relationship between the deformation field strength (controlled by σ) and the minimum Jacobian value signifying the severity of the lack of topology preservation is clearly visible in Table II. The increasing values of $H(h)$ with increasing deformation field strength indicate that the stronger the nontopology preserving quality of the initial deformation, the greater the change to be enforced for topology preservation, which also means more iterations until convergence. The results of Table II also show empirically that the serial algorithm indeed converges for random deformation fields of arbitrary strength. This suggests that for all practical purposes, the algorithm is to converge to a desired solution.

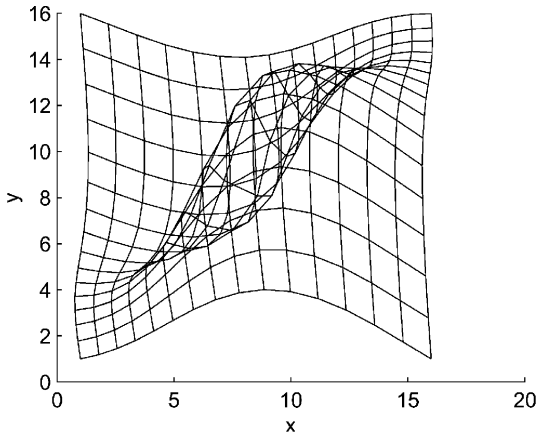

Fig. 3. Nontopology preserving deformation field h.

C. Noise Performance of the Adaptive Regularization Algorithm

In order to analyze the noise performance of the regularization aspect of the proposed technique, we have run a series of simulations where noisy observations of initial displacement fields are given

$$h = h^0 + h^n \tag{16}$$

and the true Jacobians are tightly bounded from below and above, respectively, by zero and a known upper bound. The noise displacement fields h^n are independent identically distributed from a multivariate Gaussian distribution with zero mean and covariance $\sigma^2 \mathbf{I}_2$, where $\mathbf{I}_2$ denotes the 2×2 identity matrix. The average per pixel displacement field error (in vector norm) of 20 independent runs of noisy observations h with $\sigma = 0.1, 0.2, \ldots, 1.0$, and the corresponding adaptive regularization estimates $\hat{h}$ are given in Table III.

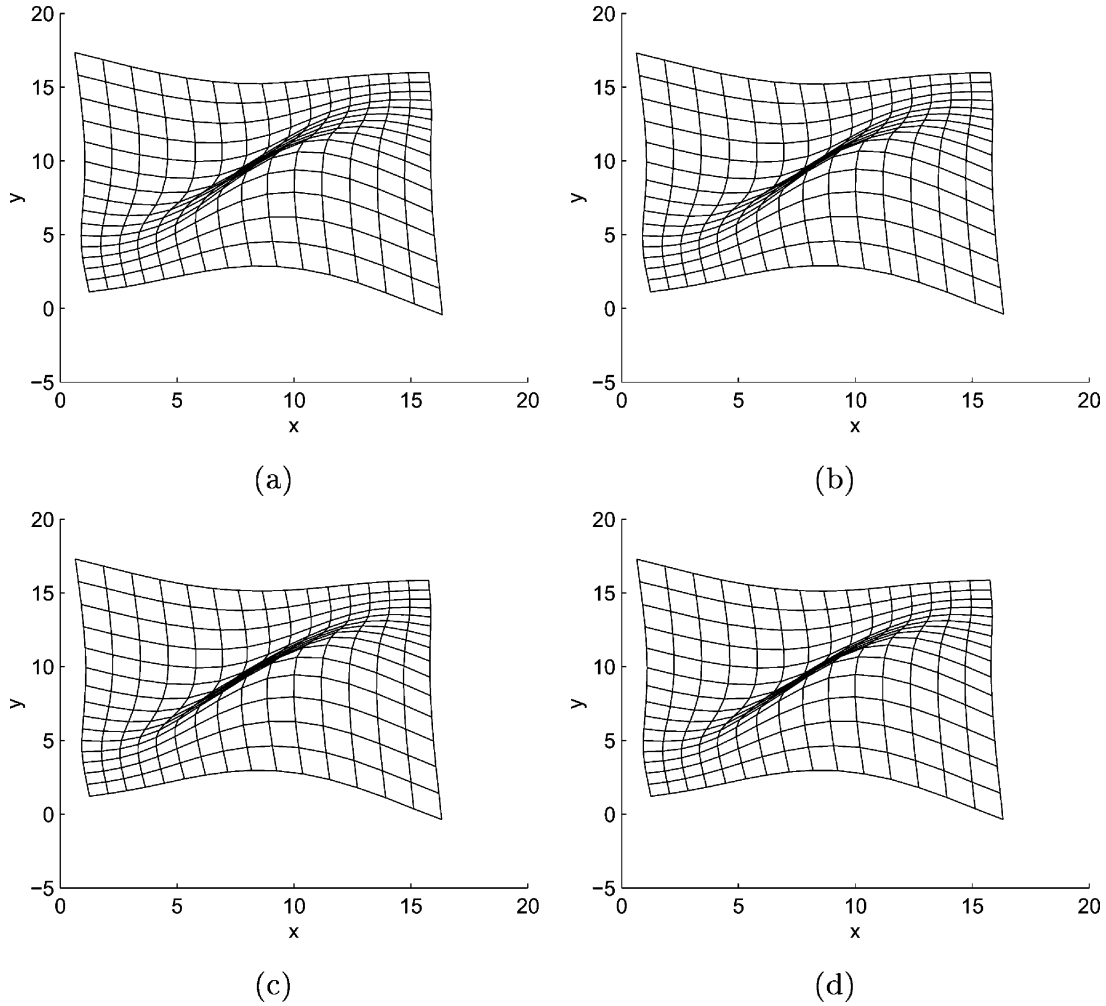

Fig. 4. Topology preserving deformation fields obtained by (a) the serial implementation (h_s), (b) the parallel implementation (h_p), (c) the optimal serial implementation (h_{os}), and (d) the optimal parallel implementation (h_{op}).

TABLE I
STATISTICS OF THE RECONSTRUCTIONS h_s, h_p, h_{os}, AND h_{op}

	h_s	h_p	h_{os}	h_{op}
iterations	9	24	16	36
error $H(h)$	0.7279	0.6930	0.6849	0.6749
minimum of Jacobians	0.057159	0.052235	0.051135	0.050977

TABLE II
CONVERGENCE ANALYSIS RESULTS FOR THE SERIAL TOPOLOGY ENFORCING ALGORITHM

σ	initial Jacobian low	final Jacobian low	iterations	cost $H(h)$
0.25	-0.4650	0.0548	10.70	0.0024
0.50	-2.7104	0.0548	17.90	0.2504
0.75	-6.6085	0.0539	20.35	1.1070
1.00	-11.7841	0.0543	22.60	2.2868
1.25	-18.8383	0.0530	24.10	3.6959
1.50	-25.9242	0.0535	25.35	5.2138
1.75	-33.9484	0.0535	26.60	7.2901
2.00	-48.1021	0.0539	27.55	8.9197
2.25	-57.4054	0.0545	28.90	11.2372
2.50	-67.7852	0.0541	28.40	13.0403
2.75	-89.7500	0.0535	28.80	15.0588
3.00	-108.7516	0.0539	29.25	17.0983

The results in Table III suggest that when the upper and lower bounds on the true Jacobians are known, the adaptive regularization technique successfully enforces these limits onto the observed noisy displacement fields. As a result, not only the issues related with topology preservation and regularity are rectified, but the observation error is also reduced.

D. Simulation Results on Synthetic and Real Medical Images

1) Two-Dimensional Results: We have also applied the described technique on synthetic and real medical images to demonstrate the corrective effect of enforcing topology preservation on a given displacement field. A 2-D synthetic brain template acquired from the *BrainWeb* database [6], the image corresponding to a deformed version of the template according to a nontopology preserving displacement field, and the deformed image obtained using the topologically corrected (with $\epsilon = 0.1$) displacement field [14] are shown in Fig. 5. The nontopology preserving characteristics of the initial displacement field are clearly visible by the interweaved morphological structures. The topology preservation enforcing algorithm accurately recovers the lost neighborhood properties.

We next illustrate the regularization aspect of the topology preservation enforcing algorithm on the Jacobians corresponding to deformation fields obtained by a boundary-based

TABLE III
ERROR PERFORMANCE OF THE ADAPTIVE REGULARIZATION ALGORITHM

σ	$\lvert h^0 - \hat{h}\rvert$	$\lvert h^n\rvert$
0.1	0.1247	0.1252
0.2	0.2471	0.2498
0.3	0.3549	0.3781
0.4	0.4333	0.4995
0.5	0.4935	0.6265
0.6	0.5218	0.7613
0.7	0.5770	0.8709
0.8	0.6087	0.9902
0.9	0.6328	1.1269
1.0	0.6481	1.2533

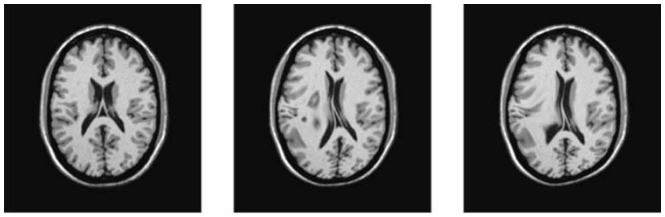

Fig. 5. Illustration of the enforced topological correction. (a) Synthetically generated 2-D brain template, (b) warped template according to a nontopology preserving displacement field, and (c) warped template according to the corrected displacement field.

elastic deformation [11] on real 2-D MRIs of corpus collosum acquired over the midsagittal plane. These images were initially analyzed in a regional volumetric difference detection framework between two groups [10]. Each group consisted of 9 subjects selected randomly with exclusion from a right-handed male population, where a systematic 50% shrinkage was simulated in the posterior part of the corpus collosum on the second group subjects. After the elastic deformation and subsequent displacement field estimation for every subject, regional atrophy was detected by a pointwise two-tailed t-test of the respective Jacobians and corresponding P values.

We analyze the effects of adaptive regularization enforced onto the initially estimated displacement fields $h = (f, g)$ to bound the resulting Jacobians within the interval $[0.2, 5] \subset \mathbb{R}$ on the atrophy detection performance in comparison with a Gaussian regularizer that tightly provides the same bounds on the Jacobians. Gaussian smoothing is the most widely used method in voxel-based morphometric analyses [2]. The error measures used in the analysis to quantify the deviation of the estimated (regularized) displacement fields $\hat{h} = (\hat{f}, \hat{g})$ from the initial values $h = (f, g)$ are the cumulative displacement field error

$$E(\hat{h}|h) = \sum_{x,y\in\Omega} \left(\left(\hat{f}(x,y) - f(x,y) \right)^2 + \left(\hat{g}(x,y) - g(x,y) \right)^2 \right)^{\frac{1}{2}} \tag{17}$$

the maximum displacement field error

$$E^{\max}(\hat{h}|h) = \max_{x,y\in\Omega} \left(\left(\hat{f}(x,y) - f(x,y) \right)^2 + \left(\hat{g}(x,y) - g(x,y) \right)^2 \right)^{\frac{1}{2}} \tag{18}$$

the cumulative gradient error

$$E'(\hat{h}|h) = \sum_{x,y\in\Omega} \left(\hat{f}_x(x,y) - f_x(x,y) \right)^2 + \left(\hat{f}_y(x,y) - f_y(x,y) \right)^2 + \left(\hat{g}_x(x,y) - g_x(x,y) \right)^2 + \left(\hat{g}_y(x,y) - g_y(x,y) \right)^2 \tag{19}$$

and the Jacobian error

$$E^J(\hat{h}|h) = \sum_{x,y\in\Omega'} \left(\frac{\hat{J}^1(x,y) + \hat{J}^3(x,y)}{2} - \frac{J^1(x,y) + J^3(x,y)}{2} \right)^2 \tag{20}$$

which measures the size difference between the respective images of the square patches in the domain. Note that the area of a warped square can easily be shown to be equal to $(J^1(x,y) + J^3(x,y))/2$ or to $(J^2(x,y) + J^4(x,y))/2$. The resulting error analysis is displayed in Table IV.

The amount of correction in the regularized displacement fields $\hat{h} = (\hat{f}, \hat{g})$ by the two regularization methods is illustrated in Fig. 6. Eventhough both regularization approaches achieve the desired bounds on the resulting Jacobians, the modification imposed by the proposed technique is highly localized while the Gaussian regularizer smoothens the displacement field uniformly. These results reveal the nature of the Gaussian regularization which acts as a low-pass filter and removes the high oscillatory components from the displacement fields. In cases where the irregularity is known to be caused by relatively weak high frequency behavior in the displacement fields, such a regularization can be expected to perform well. We know, however, by the example of Fig. 3, that the displacement fields can vary smoothly and yet be irregular to the point of violating topology preservation, in which case a Gaussian (or any low-pass oriented) regularizer would fail. The adaptive approach developed in this paper, on the other hand, accurately localizes and corrects the undesired irregular behavior in a given displacement field.

A t-test analysis similar to the one in [10] using the same dataset of 18 subjects reveals that the proposed adaptive regularization improves the atrophy detection by providing a lowest P value of 7.40 10^{-10} at the atrophy region over both the original and Gaussian regularized results with subsequent respective lowest P values of 1.86 10^{-9} and 3.52 10^{-9}. These minute P values reflect the strength of the simulated atrophy (50%), and the performance degradation by the Gaussian regularization seems to be relatively insignificant. In cases where the atrophies are much more attenuate, however, adequate regularization is of crucial importance and the benefit of the proposed adaptive approach is much more pronounced for regional volumetric change analysis.

2) Three-Dimensional Results: We first provide a comparison of deformation field corrections obtained by enforcing topology preserving regularity conditions only on the 8 corner Jacobians, and on all 64 Jacobians. We have generated random displacements on a $5 \times 5 \times 5$ regular grid by a thin plate spline interpolation on random displacements induced on the 8 corners of the domain and the center. The random deformations are generated as zero-mean Gaussian random vectors with covariances $\sigma^2 I_{3\times 3}$. The standard deviation σ is treated as the control variable that defines the strength of the deformation. For every $\sigma = 0.5, 0.6, \ldots, 1.0$, we have generated 20 random deformations and measured the average difference between

TABLE IV
CORRECTION ANALYSIS OF THE ADAPTIVE REGULARIZATION TECHNIQUE IN COMPARISON WITH A GAUSSIAN REGULARIZER FOR ALL 18 SUBJECTS

	Adaptive regularization				Gaussian regularization			
subject	E	$E^{\max}$	E'	E^J	E	$E^{\max}$	E'	E^J
1	555.40	1.19	155.87	11.18	199.96	2.04	922.15	44.58
2	187.10	0.48	32.90	3.53	114.61	1.19	408.15	22.64
3	276.43	0.64	49.43	5.01	102.79	1.63	451.53	28.31
4	245.23	0.92	42.01	3.31	96.79	1.41	342.86	18.42
5	413.74	1.48	111.59	7.28	158.18	1.97	681.37	37.19
6	366.55	1.34	88.64	9.11	204.05	2.15	804.40	45.67
7	222.34	1.51	60.34	4.87	207.65	2.43	744.83	44.28
8	274.56	0.69	34.89	3.00	144.46	1.20	523.21	22.85
9	247.34	0.70	57.15	3.96	120.71	1.14	507.32	26.16
10	257.29	0.73	57.67	3.49	148.62	1.35	610.59	24.24
11	1030.69	2.61	355.52	25.65	1112.05	4.11	2170.12	101.99
12	501.89	1.36	161.44	8.42	432.61	2.52	1207.94	42.53
13	262.32	1.05	57.76	2.64	124.89	1.39	502.73	16.65
14	332.69	1.57	87.86	4.58	353.09	2.81	908.59	34.01
15	581.53	1.47	148.17	9.35	189.88	2.21	863.07	34.71
16	590.69	1.69	184.22	10.18	636.20	2.81	1472.56	60.12
17	1442.08	3.06	329.43	26.56	1838.79	4.12	2613.09	119.52
18	1593.47	4.76	809.23	53.52	3917.99	8.26	4141.60	183.80
average	521.19	1.51	156.89	10.87	561.30	2.48	1104.23	50.43

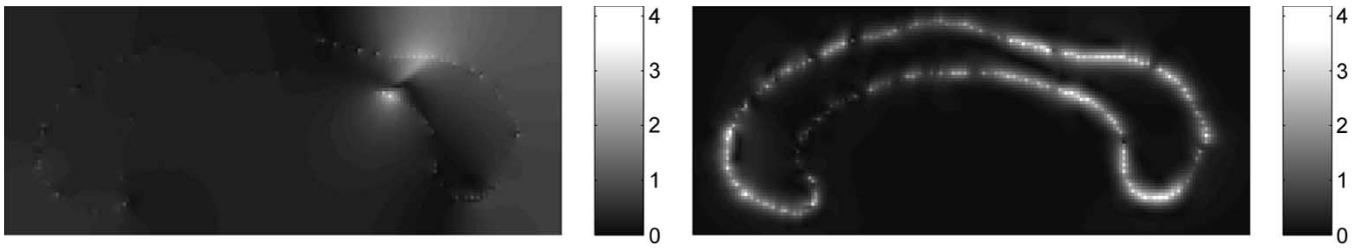

Fig. 6. Illustration of the displacement field correction on subject 17 resulting from (a) the proposed adaptive regularization technique, and (b) a Gaussian regularizer.

TABLE V
COMPARISON BETWEEN THE DEFORMATION FIELDS OBTAINED BY PROCESSING ONLY THE 8 CORNER JACOBIANS AND BY PROCESSING ALL 64 JACOBIANS. THE ORIGINAL DEFORMATION FIELDS ARE DENOTED BY h, THE CORRECTED DEFORMATION FIELDS BY PROCESSING THE CORNER JACOBIANS AND ALL 64 JACOBIANS ARE DENOTED BY $\hat{h}_8$ AND $\hat{h}_{64}$, WHILE THE CORRESPONDING COMPUTATION TIMES IN SECONDS ARE DENOTED BY t_8 AND t_{64}. THE TERMS $d(h, \hat{h}_8)$, $d(h, \hat{h}_{64})$ AND $d(\hat{h}_8, \hat{h}_{64})$ REPRESENT THE AVERAGE VOXEL-WISE DISTANCE OF THE INDICATED DEFORMATION FIELDS IN TERMS OF THE UNIT GRID SPACING. POSITIVITY OF CORNER JACOBIANS IS NECESSARY FOR TOPOLOGY PRESERVATION IN THREE DIMENSIONS, WHILE POSITIVITY OF ALL 64 JACOBIANS IS SUFFICIENT. EACH LINE REPRESENTS THE AVERAGE OF 20 REPEATS

σ	range of initial corner Jacobians	t_8	t_{64}	$d(h, \hat{h}_8)$	$d(h, \hat{h}_{64})$	$d(\hat{h}_8, \hat{h}_{64})$
0.5	[-0.2697, 3.1549]	0.6901	8.9332	0.0341	0.0445	0.0143
0.6	[-0.6728, 3.5877]	0.9336	13.2748	0.0743	0.0977	0.0334
0.7	[-1.3029, 4.7819]	1.3269	18.8899	0.1405	0.1730	0.0479
0.8	[-1.3506, 4.9864]	1.6171	20.2030	0.1911	0.2340	0.0641
0.9	[-1.8332, 6.4200]	1.6232	21.3560	0.2534	0.3119	0.0853
1.0	[-2.5176, 7.0301]	2.0279	25.2166	0.3419	0.4046	0.1003

the deformation corrections obtained by confining the corner Jacobians to the interval [0.25, 4.00] and the deformation correction obtained by confining all 64 Jacobians to the same interval. Table V summarizes the statistics of the simulations as well as the computation times and the average distance between resulting deformation fields from both strategies.

The results suggest that even when the initial deformations are very strong, the average difference between the deformation fields obtained by correcting only the corner Jacobians and all 64 Jacobians is consideraby smaller than the average corrections imposed on the deformation fields, and remains an order of magnitude smaller than the unit distance grid spacing. On the other hand, the computational cost of correcting all Jacobians is roughly 10 times the cost of correcting only the corner Jacobians, which indicates that processing only the corner Jacobians is a reasonable approximation.

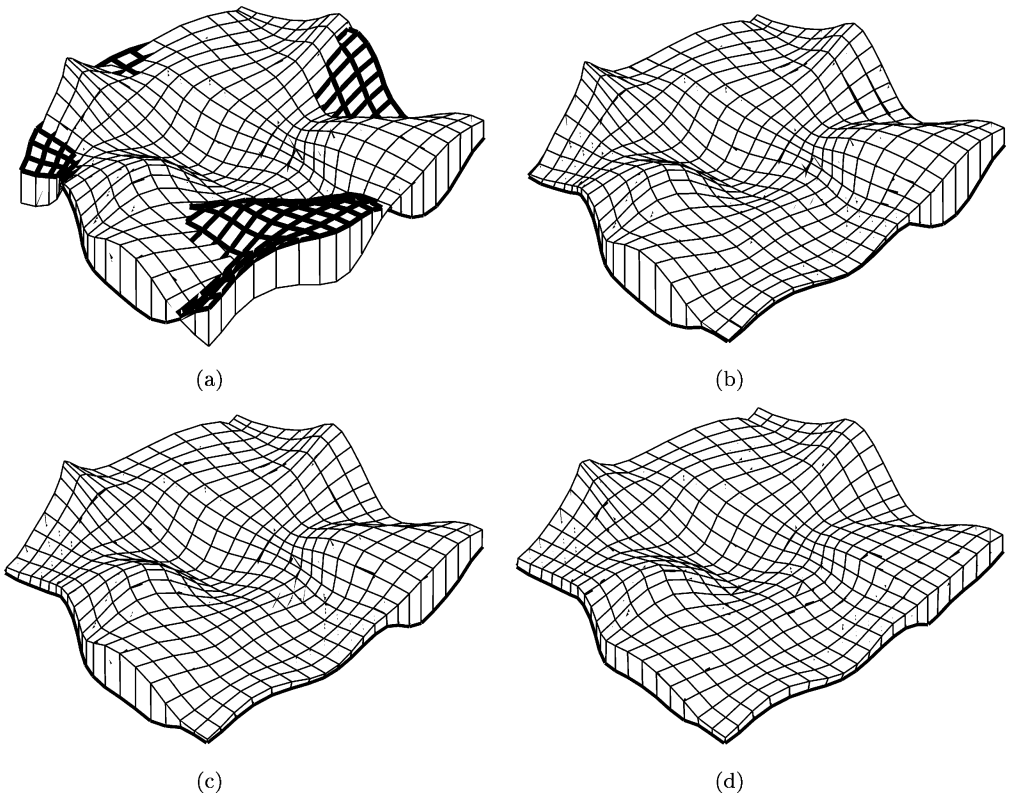

Fig. 7. Illustration of the regularization aspect of the proposed algorithm. The deformation field in (a) has corner Jacobian values within $[-5.8915, 6.4762]$. The lower level grid is represented by darker lines which protrude through the upper level grid in violation of topology preservation. The deformation fields in (b), (c) and (d) are obtained by applying the proposed algorithm to the original deformation field by restricting the corner Jacobians, respectively, to the intervals [0.1, 10.0], [0.3, 5.0], and [0.5, 2.5]. As the range of the interval diminishes, the resulting deformation field becomes more and more regular while the deformation features are preserved to a great extent.

In order to demonstrate the adaptive regularization aspect of the proposed algorithm, we have generated a $21 \times 21 \times 2$ random deformation field that exhibits folds and, thus, does not preserve topology. We have then applied the adaptive regularization method to confine the corner Jacobians to within the intervals [0.1, 10.0], [0.3, 5.0], and [0.5, 2.5]. The resulting deformation fields together with the original nontopology preserving deformation field are shown in Fig. 7. In order to highlight the violation of topology preservation, the lines of the lower grid are drawn four times darker than the others. In the original deformation field, the lower slice grid clearly crosses over the upper slice grid, and violates topology preservation conditions. In the deformation fields obtained by restricting the corner Jacobians to the respective intervals, these folds are corrected and topology preservation is achieved. Furthermore, as the intervals gradually shrink into smaller neighborhoods of 1, the overall deformation becomes more and more regular, since marginal Jacobian values associated with large expansions and contractions are pulled toward more moderate levels.

We have also applied the topology preservation technique to a set of deformation field estimates that register 3-D MRI scans of 158 patients to a predefined template. The deformation fields have been obtained using a previously documented voxel-wise registration technique [18], [19], which employs its own smoothness considerations on the computed deformation fields. Using the proposed method, we have enforced the corner Jacobians of these deformations to be within the interval [0.1,7.0]. Out of these 158 deformation fields, 17 readily satisfied these bounds over the template which resides within a neighborhood of size $149 \times 183 \times 141$. The statistics of the computation times of bringing the initial Jacobians within this range for the remaining 141 is shown in Table VI. The block size is the size of the blocks over which integrability is applied individually and repeated 7 times globally within the second step of the serial implementation (the integrability step). Larger block sizes imply wider dissemination of the integrability information at the expense of increased computational cost. The implementation was made in C (the code is available upon request) and run on a Silicon Graphics Inc. 8-cpu Origin 300 server with 4 GBytes of RAM. The effect of the topology preserving regularization on one such deformation field is shown in Fig. 8. The initial deformation field has irregularities which are produced as artefacts of the voxel-wise registration algorithm. The regularized deformation field smoothens over these artefacts with high fidelity to the registration.

TABLE VI
THE STATISTICS OF THE COMPUTATION TIME (IN SECONDS) TO BRING THE JACOBIANS OF 141 REAL DEFORMATION FIELDS TO WITHIN THE INTERVAL [0.1,7.0]. READING A $149 \times 183 \times 141$ DEFORMATION FIELD, CHECKING TO SEE WHETHER IT COMPLIES WITH THESE BOUNDS AND WRITING IT BACK ONTO THE DISK TOOK AN AVERAGE OF 48.16 s

block size	3	4	5	6
mean	172.62	247.31	432.15	795.92
standard deviation	54.97	104.72	235.45	474.29
median	167.40	225.60	365.60	673.90

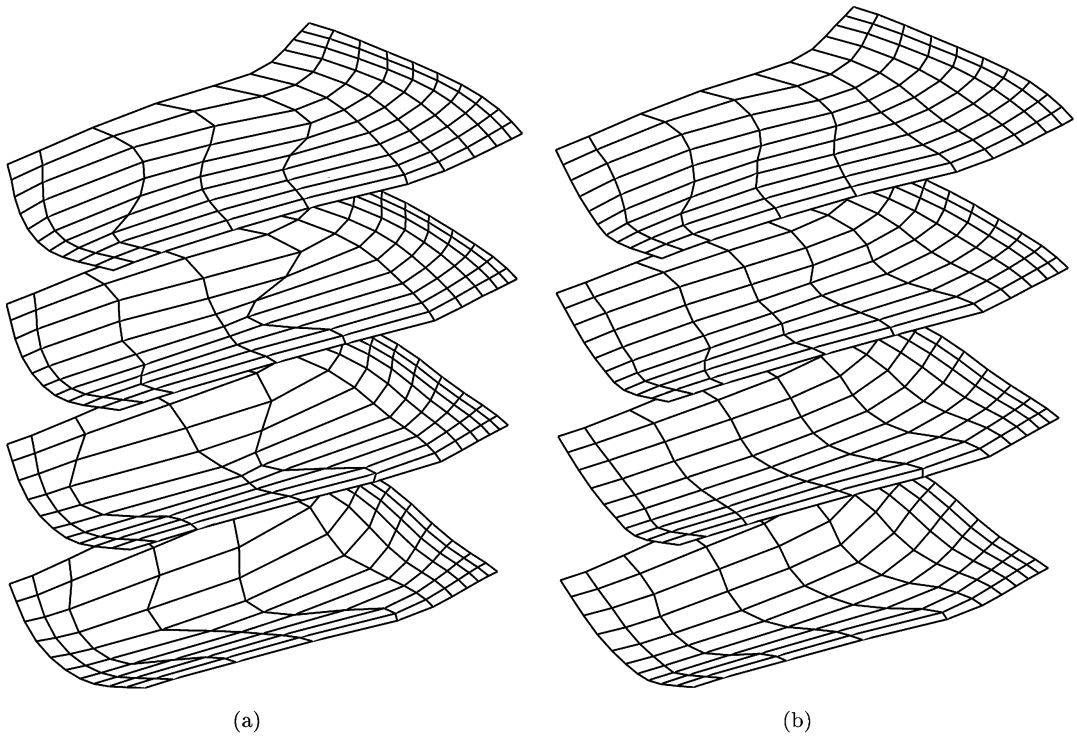

Fig. 8. Effect of topology preserving adaptive regularization on real deformation fields. The deformation in (a) is the result of a voxel-wise image matching method, shown only a $11 \times 11 \times 4$ block with disjoint slices. Confining the corner Jacobians to an interval of [0.2, 5.0] produces the deformation field in (b) which is more regular in terms of the grid lines and is also true to the original registration.

The results in Table VI clearly show that with the block processing techniques, the proposed scheme to enforce topology preservation and regularity constraints on a given regular size 3-D deformation field is feasible and acceptable in the larger scale of a registration problem. It should be noted that the results represent correction times on an alternatively regularized deformation fields, which do not require extensive modifications to comply with the Jacobian bounds. The computation times will be larger for cases where a significant portion of the corner Jacobians violate the prescribed bounds. We have, however, observed that correcting a deformation field to achieve tighter bounds which required around 80 000–100 000 corner Jacobian corrections at the very first iteration typically takes around 10–15 min, which is still feasible in a voxel-wise registration scheme.

V. Conclusion

In this paper, we have presented a generic scheme to enforce topology preservation constraints on a given deformation field. Specifically, we have described the set of constraints that a discrete deformation field needs to satisfy in order to generate a topology-preserving continuous counterpart after linear interpolation. Then, we have described an iterative algorithm to enforce these constraints as bounds on the Jacobians on a given deformation field. We have also discussed that the nature of the prescribed bounds on the Jacobians serve not only to achieve topology preservation, but also a desirable kind of adaptive regularity, which effectively limits the allowed expansions and contractions of the template when it is fitted over a subject scan.

The simulation results on both synthetic and real data indicate that even in the absence of theoretical guarantees of optimality, the algorithm achieves the desired bound on the Jacobians with much less modification than a Gaussian regularizer. The adaptive nature of the algorithm allows it to address the violations locally and undo the folds without disrupting the surrounding regions unnecessarily. Due to the integrability step in the algorithm, the computational expense in regular size 3-D deformation fields grows large, but can still be handled in a feasible manner thanks to block processing implementations.

The proposed technique is general in character due to the arbitrary manifestations of the discrete deformation fields and, thus, is free from model-specific limitations. Furthermore, as it provides enforcing topology preservation as a hard constraint on a given deformation field with minimal corrections, it allows relaxing the run-time constraints of similar nature which holds a great potential in improving the registration schemes in their choices toward maximizing image similarity criteria. Notably, the proposed algorithm can be applied to intermediate estimates of the final deformation field as well as the final estimate itself. The adaptive nature of the algorithm would then identify the regions where the established matches are feasible and unfeasible in terms of topology preserving regularity criteria, and update the current estimate over the problematic regions while maintaining the highest fidelity over the remaining areas. The computation times presented in Table VI indicate that the algorithm can indeed be called several times during a voxel-wise deformable registration procedure without a significant increase in the computational burden.

An additional benefit of the algorithm stems from its ability to characterize deformation fields based on their topology

preserving regularity properties. In a general image matching framework, one of the essential challenges is to determine the best point correspondences out of a multitude of possibilities. The combinations of different possible matches at all points in the domain produces displacement field candidates, among which the best one (according to some criterion) is to be determined. In this context, our approach can also be used to characterize these candidate displacement fields based on their topology preserving and smoothness characteristics, which can act as a very resourceful discriminative tool in deciding for the deformation direction toward which to advance. This would lead to a general algorithm to determine point correspondences from a multiplicity of possibilities according to regularity and topology preservation criteria.

APPENDIX

A. Jacobian Determinant Inside a Cubic Patch

Let a deformation field h be defined in terms of its Cartesian components f, g, and e over the unit cube as a tri-linear interpolation of a set of deformations defined on the vertices. Let the deformation at vertex (i,j,k) be given as $h_{ijk} = [f_{ijk}\ g_{ijk}\ e_{ijk}]^T$ for all other vertices i, j, $k = 0$, 1. The deformation field at a point (x,y,z) inside the unit cube is then given as

$$\begin{aligned} f(x,y,z) = {} & (1-z)\left((1-y)\left((1-x)f_{000} + xf_{001}\right)\right. \\ & \left. + y\left((1-x)f_{010} + xf_{011}\right)\right) \\ & + z\left((1-y)\left((1-x)f_{100} + xf_{101}\right)\right. \\ & \left. + y\left((1-x)f_{110} + xf_{111}\right)\right) \end{aligned}$$

and similarly for $g(x,y,z)$ and $e(x,y,z)$. The Jacobian matrix of h at (x,y,z) is then

$$J = [\mathbf{c}_1 \quad \mathbf{c}_2 \quad \mathbf{c}_3] \tag{21}$$

where the column vectors $\mathbf{c}_1$, $\mathbf{c}_2$, and $\mathbf{c}_3$ are given by

$$\begin{aligned} \mathbf{c}_1 = {} & (1-z)\left((1-y)(\Delta_x h_{00}) + y(\Delta_x h_{01})\right) \\ & + z\left((1-y)(\Delta_x h_{10}) + y(\Delta_x h_{11})\right) \\ \mathbf{c}_2 = {} & (1-z)\left((1-x)(\Delta_y h_{00}) + x(\Delta_y h_{01})\right) \\ & + z\left((1-x)(\Delta_y h_{10}) + x(\Delta_y h_{11})\right) \\ \mathbf{c}_3 = {} & (1-y)\left((1-x)(\Delta_z h_{00}) + x(\Delta_z h_{01})\right) \\ & + y\left((1-x)(\Delta_z h_{10}) + x(\Delta_z h_{11})\right) \end{aligned}$$

with $\Delta_x h_{ij} = h_{ij1} - h_{ij0}$, $\Delta_y h_{ij} = h_{i1j} - h_{i0j}$, and $\Delta_z h_{ij} = h_{1ij} - h_{0ij}$ for i, $j = 0$ and , 1. Now, the determinant of J, denoted by $|J|$, can be expanded as

$$\begin{aligned} |J| = {} & (1-z)\left((1-y)|\Delta_x h_{00}\ \ \mathbf{c}_2\ \ \mathbf{c}_3| + y|\Delta_x h_{01}\ \ \mathbf{c}_2\ \ \mathbf{c}_3|\right) \\ & + z\left((1-y)|\Delta_x h_{10}\ \ \mathbf{c}_2\ \ \mathbf{c}_3| + y|\Delta_x h_{11}\ \ \mathbf{c}_2\ \ \mathbf{c}_3|\right). \end{aligned}$$

Note that the expansion of $\mathbf{c}_1$ replaced the determinant $|J|$ with a linear combination of four determinants. Replacing the expressions for $\mathbf{c}_2$ and $\mathbf{c}_3$ results in

$$|J| = \sum_{i,j=0}^{1} \sum_{k,l=0}^{1} \sum_{m,n=0}^{1} \alpha_{ijklmn} |\Delta_x h_{ij}\ \ \Delta_x h_{kl}\ \ \Delta_x h_{mn}| \tag{22}$$

where α_{ijklmn} is the appropriate coefficient. Note that this expansion now consists of a total of 64 terms, among which only 8 correspond to the corner Jacobians.

B. Reconstructing Functions From Nonintegrable Gradient Fields

Let f be a real valued function defined over a 3-D regular grid denoted by Ω, $f : \Omega \to \mathbb{R}$. Let also $\bigtriangledown f$ denote the gradient field of f, $\bigtriangledown f : \Omega \to \mathbb{R}^3$. Note that $\bigtriangledown f$ can be computed by either a finite differences approximation or an alternative kernel-type estimator. In any case, the operator O defined by

$$O(f) = \bigtriangledown f = (f_x, f_y, f_z) \tag{23}$$

is linear, where the superscript denotes partial derivative approximation along the indicated direction. The problem of reconstructing an unknown function f from its gradient field (f_x, f_y, f_z) then corresponds to inverting the operator O. This, however, is an ill-posed problem since the dimensionality of (f_x, f_y, f_z) is roughly three times the dimensionality of f, unless the gradient field (f_x, f_y, f_z) is integrable, i.e., integrating the gradient field does not depend on the integration path. On the other hand, a deeper understanding of the problem is needed if this is not the case.

Consider the enumerated set of functions $\{f_i\}$ for $i = 1, \ldots, n$, and suppose that they constitute a basis for the space of real-valued functions

$$\mathcal{F} = \{f |\ f : \Omega \to \mathbb{R}\}. \tag{24}$$

The gradients of these basis functions $O(f_i) = (f_x, f_y, f_z)_i$ then span a k-dimensional subspace of the gradient space S which is the subspace of integrable gradient fields. Note that $k < n$ since the gradient operator, no matter how it is implemented, always removes the constant component from the functions. An orthonormal basis for S can easily be constructed by orthonormalizing $\{(f_x, f_y, f_z)_i\}$ to obtain $\{\overline{(f_x, f_y, f_z)}_j\}$ together with $\overline{f}_j = O(\overline{(f_x, f_y, f_z)}_j)$ for $j = 1, \ldots, k$. Given a gradient field (f_x, f_y, f_z), the function $\hat{f}$ given by

$$\hat{f} = \sum_j \left\langle (f_x, f_y, f_z), \overline{(f_x, f_y, f_z)}_j \right\rangle \overline{f}_j \tag{25}$$

then solves $O(f) = (f_x, f_y, f_z)$. Furthermore, it provides the minimum norm solution to this inverse problem in the space of gradient fields, since it characterizes a projection onto the feasible subspace.

C. Large-Scale Implementation Issues and Block Processing Solutions

The algorithm described above implements a vector space projection, and hence, is very fast. On the other hand, it requires precomputation of the sets $\{\overline{f}_j\}$ and $\{\overline{(f_x, f_y, f_z)}_j\}$ and the size of these sets as well as the amount of required memory grows rapidly with the size of Ω. In order to implement this algorithm on real-sized deformation fields, block processing techniques are required.

One approach is to divide the domain Ω into nonoverlapping blocks, enforce integrability on these blocks individually, and compute constant shifts for each block in a way to minimize some measure of inconsistency across block boundaries [16]. This method is fast since it requires only a single pass across the domain, but propagates the integrability information only within a single block. Another option is to partition Ω into overlapping blocks, and enforce integrability as described above onto each

and every block for multiple passes. This approach takes longer, but has the advantage of extending the integrability information across the whole domain, and can be shown to converge to the global solution asymptotically. In our implementation, we choose the second option since we have observed the gradient field correction due to topology preservation to be highly localized, so that repeated passes was not computationally prohibitive, and we could approach the global solution within six passes overall. It should also be noted that the integrability is to be enforced only on those blocks which have been modified by the preceding gradient field correction step or the previous pass of integrability enforcement. The results of Table VI have been obtained by a C implementation of the topology preservation algorithm without further code optimization for speed.

REFERENCES

[1] J. Ashburner, J. L. R. Andersson, and K. J. Friston, "High-dimensional image registration using symmetric priors," *NeuroImage*, vol. 9, no. 6, pp. 619–628, 1999.

[2] J. Ashburner and K. J. Friston, "Voxel-based morphometry: the methods," *NeuroImage*, vol. 11, no. 6, pp. 805–821, 2000.

[3] J. Ashburner, P. Neelin, D. L. Collins, A. Evans, and K. J. Firston, "Incorporating prior knowledge into image registration," *Neuroimage*, vol. 6, pp. 344–352, 1997.

[4] F. L. Bookstein, "Principal warps: thin-plate splines and the decomposition of deformations," *IEEE Trans. Pattern Anal. Machine Intell.*, vol. 11, pp. 567–585, June 1989.

[5] G. E. Christensen, R. D. Rabbitt, and M. I. Miller, "Deformable templates using large deformation kinematics," *IEEE Trans. Image Processing*, vol. 5, pp. 1435–1447, Oct. 1996.

[6] C. Cocosco, V. Kollokian, R.-S. Kwan, and A. Evans, "Brainweb: online interface to a 3D MRI simulated brain database," in *Proc. 3rd Int. Conf. Functional Mapping of the Human Brain*, vol. 5, 1997, p. 4.

[7] P. L. Combettes, "The foundations of set theoretic estimation," *Proc. IEEE*, vol. 81, pp. 182–208, Feb. 1993.

[8] ——, "Signal recovery by best feasible approximation," *IEEE Trans. Image Processing*, vol. 2, pp. 269–271, Feb. 1993.

[9] C. Davatzikos, "Spatial normalization of 3d brain images using deformable models," *J. Comput. Assist. Tomogr.*, vol. 20, no. 4, pp. 656–665, 1996.

[10] ——, "Measuring biological shape using geometry-based shape transformations," *Image Vis. Computing*, vol. 19, pp. 63–74, 2001.

[11] C. Davatzikos, M. Vaillant, S. M. Resnick, J. L. Prince, S. Letovsky, and R. N. Bryan, "A computerized approach for morphological analysis of the corpus collosum," *J. Comput. Assist. Tomogr.*, vol. 20, no. 1, pp. 88–97, 1997.

[12] K. J. Firston, J. Ashburner, C. D. Frith, J.-B. Poline, J. D. Heather, and R. S. J. Frackowiak, "Spatial registration and normaliza-tion of images," *Human Brain Mapping*, vol. 2, pp. 165–189, 1995.

[13] H. J. Johnson and G. E. Christensen, "Landmark and intensity based, consistent thin-plate spline image registration," in *Lecture Notes in Computer Science*, M. F. Insana and R. M. Leahy, Eds. Berlin, Germany: Springer, 2001, vol. 2082, Proc. Int. Conf. Information Processing in Medical Imaging, pp. 329–343.

[14] B. Karaçalı and C. Davatzikos, "Topology preservation and regularity in estimated deformation fields," in *Proc. 18th Int. Conf. Information Processing in Medical Imaging*, 2003, pp. 426–437.

[15] B. Karaçalı and W. Snyder, "Partial integrability in surface reconstruction from a given gradient field," in *Proc. IEEE Int. Conf. Image Processing*, vol. 2, 2002, pp. 525–528.

[16] ——, "Reconstructing discontinuous surfaces from a given gradient field using partial integrability," *Comput. Vis. Image Understanding*, vol. 92, no. 1, pp. 78–111, 2003.

[17] O. Musse, F. Heitz, and J.-P. Armspach, "Topology preserving deformable image matching using constrained hierarchical parametric models," *IEEE Trans. Image Processing*, vol. 10, pp. 1081–1093, July 2001.

[18] D. Shen and C. Davatzikos, "Very high resolution morphometry using mass-preserving deformations and hammer elastic registration," *NeuroImage*, vol. 18, no. 1, pp. 28–41, 2003.

[19] D. Shen, E. H. Herskovits, and C. Davatzikos, "An adaptive-focus statistical shape model for segmentation and shape modeling of 3-D brain structures," *IEEE Trans. Med. Imag.*, vol. 20, pp. 257–270, Aug. 2001.

[20] J.-P. Thirion, "Image matching as a diffusion process: an analogy with maxwell's demons," *Med. Image Anal.*, vol. 2, no. 3, pp. 243–260, 1998.

[21] H. J. Trussell and M. Civinlar, "The feasible solution in signal restoration," *IEEE Trans. Acoust., Speech, Signal Processing*, vol. ASSP-32, pp. 201–212, Apr. 1984.